IEEE Access
Multidisciplinary | Rapid Review | Open Access Journal

Received January 7, 2021, accepted January 17, 2021, date of publication January 20, 2021, date of current version February 1, 2021.

Digital Object Identifier 10.1109/ACCESS.2021.3053080

An Optimized Permanent Magnet Brake Mechanism in Robot Joints

KAIMENG WANG[1], HEHUA JU[1,2,3], YANG YANG[1], AND ZHENHAO GUO[1]
[1]College of Astronautics, Nanjing University of Aeronautics and Astronautics, Nanjing 210000, China
[2]Key Laboratory of Ministry of Industry and Information Technology, Nanjing 210000, China
[3]Laboratory of Aerospace Entry, Descent and Landing Technology, Nanjing 210000, China

Corresponding author: Hehua Ju (juhehua@nuaa.edu.cn)

This work was supported by the National Natural Science Foundation of China under Grant 61673010.

ABSTRACT This paper proposes a novel brake mechanism in robot joints, especially for space robot joints which require low power consumption and high reliability. The key point of the brake mechanism is that the torque spring is replaced with the Nd-Fe-B permanent magnet. Due to the position and force relationship between the permanent magnet and the electromagnet in the brake mechanism, the stroke of the brake armature can be extended so that the bolt type brake structure is adapted and the braking torque can be infinite theoretically. Meanwhile, the holding current in the electromagnet can be decreased to save energy and reduce heat generation. The magnetic circuit models of the electromagnet and permanent magnet in the brake mechanism are established and analyzed. In order to improve the response speed of the brake mechanism, a novel H-bridge brake power supply circuit is proposed. To verify the benefits of the design, a permanent magnet brake prototype with the H-bridge power supply circuit is set up. While the holding current is consistent with the peak current in the conventional torque spring motor brake, the proposed permanent magnet brake mechanism can decrease the holding current below 0.1 A.

INDEX TERMS Brake mechanism, permanent magnet, robot joint, low power consumption.

I. INTRODUCTION

The motor brake mechanism is one of the most important parts in robot joints. It is used to ensure that the robot joints are kept at rest after power-off or emergency braking in the event of a power failure. Most of the brake designs use the torque spring to press the brake armature and the friction plate to generate the braking torque [1]–[3]. This kind of brake is also called ''power-off'' brake and mainly consists of torque springs, electromagnet, brake plate and the friction plate. The classic torque spring brake structure is shown in Fig. 1.

The spring-friction brake structure mainly consists of a stator and rotor [4], [5]. The stator part is an electromagnet which is fixed together with the stationary part of the joint, the rotor part is the friction plate connected with the motor shaft by a square rotor core. The torque spring is embedded in the electromagnet and the spring force interacts with the electromagnet suction force to control the rotation of the motor shaft [6]–[10].

The associate editor coordinating the review of this manuscript and approving it for publication was Jinquan Xu.

In order to further study the structure and working principle of the spring-friction brake, Figure. 2 illustrates the two working states of the conventional spring-friction brake device.

The working principle of this brake is as follows:

1) When the stator coil is energized, the brake armature will be attracted by the electromagnetic force to overcome the torque spring thrust and stay close to the electromagnet surface. The motor rotor shaft connected with the friction plate will be allowed to rotate freely in the air gap.

2) When the stator coil is switched off, the torque spring will press the brake armature towards the friction plate. The braking torque generated by the friction force will obstruct the rotation.

The braking torque of the spring-friction brake device can be expressed as:

$$T_{brake} = u_k \times n \times (k \times h) \times r \tag{1}$$

where u_k is the coefficient of dynamic friction between the friction plate and the brake armature, k is the stiffness coefficient of the spring, h is the compression of the spring, and n is the number of springs, r is the radius of the brake armature.

In order to optimize the joint brake to save power and reduce heat generation, this paper proposes a novel brake

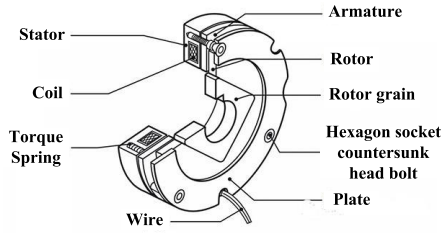

FIGURE 1. Classic torque spring brake structure.

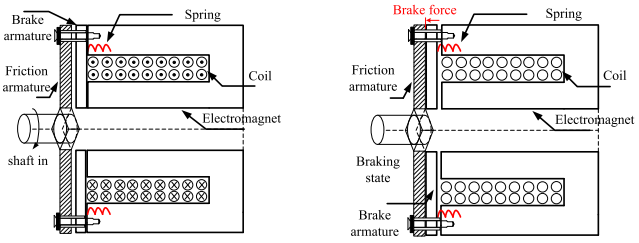

FIGURE 2. Working states of conventional spring-friction brake.

structure utilizing the permanent magnet instead of the torque spring, which has the two most important advantages:

1. Theoretically infinite braking force;
2. Low power consumption in electrical holding state;

Section II presents the proposed permanent magnet brake mechanism and illustrates the basic working principle and magnetic circuit models. Section III validates the magnetic circuit model by finite element simulation and experiment. Section IV proposes the improved brake power supply circuit. Section VI demonstrates the experimental results and provides a brief conclusion.

II. ANALYSIS OF PROPOSED BRAKE MECHANISM

A. PROPOSED BRAKE MECHANISM

In order to achieve the characteristics of large braking torque and low power consumption, permanent magnets are used to replace the torque spring in the brake mechanism. Contrary to the conventional brake structure where the torque spring is embedded in the electromagnet, permanent magnet and the electromagnet are distributed on both sides of the brake armature in the proposed brake mechanism. The force of the torque spring is inversely proportional to the stroke of the brake armature in the conventional brake mechanism which limits the armature stroke to a very small value while the permanent magnet brake shows the opposite characteristic. Table 1 lists the comparison of the working characteristics between torque spring brake and permanent magnet brake mechanism.

In Figure. 3, the proposed brake is a hollow circular ring structure to adapt to joint routing. When the brake armature is attracted to the permanent magnet, the teeth of the rotor will be jammed and a structural brake torque is generated.

TABLE 1. Comparison between torque spring and permanent magnet brake mechanism.

Parameters	Torque spring brake	Permanent magnet brake
Braking torque	normal	large
Reliability	spring fatigue problem	high reliability
Size/cost	better	normal
Power consumption	high	low

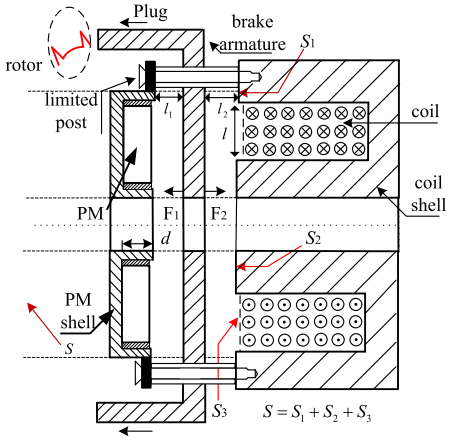

FIGURE 3. Proposed permanent magnet brake mechanism.

Figure. 3 shows the section view of the proposed permanent magnet brake mechanism in detail.

The distance from the permanent magnet to the brake armature and between the electromagnet and armature is l_1 and l_2 respectively. The sum of l_1 and l_2 is the stroke of the brake armature. The suction force of the permanent magnet and the electromagnet is marked as F_1 and F_2. The surface area of the electromagnet is marked as S which consists of three parts: the upside area of the electromagnet ring S_1 and the lower side area S_2 along with the S_3 which is the coil surface area.

The working principle of this permanent magnet brake can be described as three working states:

1) When the robot system is powered off, the brake armature will be attracted by the permanent magnet to jam the teeth of the rotor connected with the motor shaft and joint will the robot joint braking state will be achieved.

2) When the robot system is powered on, the brake power supply circuit provides an instantaneous high current pulse in the electromagnet coil to release the brake state and keep the brake armature attached to the surface of the electromagnet, so that the motor rotor can rotate freely.

3) After the motor brake is released, the brake mechanism will enter into a holding state, a small enough current of the electromagnet coil will be required to balance the permanent magnet force acting on the brake armature.

The brake mechanism working state can be adjusted by the electromagnet coil current, a further analysis of the force of the electromagnet and the permanent magnet on the brake

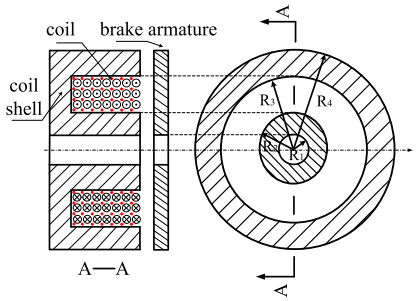

(a) Section and front view of electromagnet

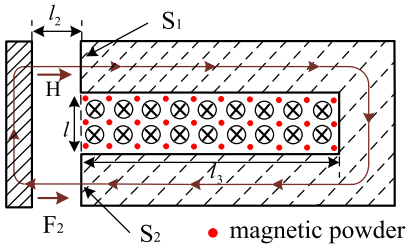

(b) Electromagnet magnetic circuit model

FIGURE 4. Section view and magnetic circuit model of electromagnet.

armature will help to further understand the working mechanism of the proposed brake.

B. MODELING OF ELECTROMAGNET MAGNETIC CIRCUIT

The electromagnet in the conventional brake mechanism is designed as a cylindrical shape with an inner and outer iron core wrapped sandwiched in the inner and outer iron core. In the space robot joints, in order to facilitate the hollow routing, the brake structure is designed as a ring shape. The electromagnet coil is filled with magnetic powder to enhance the attractive force of the electromagnet. Figure. 4 (a) shows the section and front view of the electromagnet in the proposed brake mechanism and the equivalent magnetic circuit of the brake electromagnet is given in Fig. 4 (b).

According to Figure. 4 (b), the red marked magnetic circuit from the electromagnet shell to the air gap and brake armature can be derived from the full-current ampere loop theorem [11]:

$$\oint_L H \cdot dl = \sum \left(i + \varepsilon_0 \times \frac{d\Phi_E}{dt} \right) \tag{2}$$

Ignoring the flux leakage and the iron core magnetic potential drop, the magnetic potential drop derived by the coil currents is mainly concentrated in the air gap. The magnetic flux intensity B_c generated by coil currents in the air gap is as follows:

$$B_c = \frac{u_0 \times N_c \times i}{2 \times l_2} \tag{3}$$

where N_c is the electromagnet coil turns, i is the coil current and l_2 is the length of air gap. The electromagnetic flux is uniformly distributed on the upper and lower armature surface S_1 and S_2. Therefore, the suction force of the electromagnet on

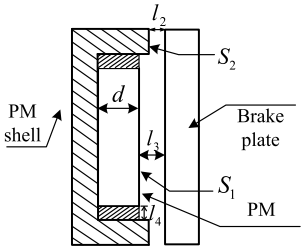

(a) Permanent magnet structure model

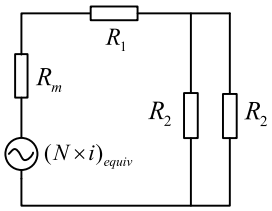

(b) Equivalent magnetic circuit

FIGURE 5. Permanent magnet structure model and equivalent magnetic circuit.

the brake armature is:

$$F_2 = \frac{B_c^2 \times (S_1 + S_2)}{2 \times u_0} \tag{4}$$

In the unsaturated magnetic circuit case, considering the magnetic potential drop on the brake armature and electromagnet iron core, the actual suction force magnitude is about 90%-95%, the coefficient k can be added, the electromagnet suction force on the brake armature can be derived as follows:

$$F_2 = \frac{k \times u_0 \times N_c^2 \times i^2 \times (S_1 + S_2)}{2 \times l_2^2} \tag{5}$$

C. MODELING OF PERMANENT MAGNET MAGNETIC CIRCUIT

The permanent magnet used in the proposed brake mechanism is an axially magnetized circular ring Nd-Fe-B permanent magnet which has the feature of extremely high magnetic energy product and high coercive force. A back iron yoke is added on the magnetizing surface of the permanent magnet to regularize the magnetic circuit to enhance the suction force. Figure. 5 is the permanent magnet model in the proposed brake mechanism and the equivalent magnetic circuit of the permanent magnet structure [12].

In Fig. 5 (a), d is the length of the magnetizing direction of the permanent magnet, l_3 is the distance between the permanent magnet and the brake armature and l_2 is the distance between the permanent magnet back iron and the brake armature. l_3 should be a little larger than l_2, so that the direct collision between the permanent magnet and the brake armature can be avoided. S_1 is the area in the magnetizing direction of the permanent magnet and S_2 is the edge area of the permanent magnet back iron cover on the magnetic circuit. There is an air gap l_4 between the permanent magnet and the back iron in the radical direction, this air gap has the following two functions:

1. Used to fill the glue to fix the permanent magnet;
2. Weakening the magnetic flux leakage of the permanent magnet from the N pole to the S pole directly through the back iron;

The magnetization curve of the Nd-Fe-B permanent magnet in the second quadrant which is also the effective working range is approximately linear. Figure. 6 (a) describes the

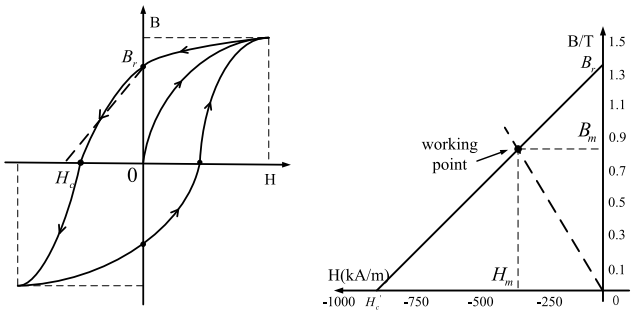

(a) 4-quadrant magnetization curve

(b) Magnetization curve in second quadrant

FIGURE 6. Permanent magnet magnetization curve.

magnetization curve of the permanent magnet and the approximately linear magnetization curve in the second quadrant is given in Fig. 6 (b) [13].

Assuming that the DC magnetization curve of the Nd-Fe-B permanent magnet is linear in second quadrant, the DC magnetization curve of the Nd-Fe-B permanent magnet in second quadrant can be expressed as:

$$B = u_R \times \left(H - H_c'\right) = B_r + u_B \times H \tag{6}$$

where H_c' is the apparent coercive force related to the curve which is slightly larger than the coercive force of the material in value. u_R is the slope of the curve and the standard value is close to air permeability. The working point (H_m, B_m) of the Nd-Fe-B permanent magnet can be derived from Eq. 6.

The working point of the permanent magnet can be derived by the equivalent magnetic circuit model or the magnetic flux continuity theorem. The calculation results of the two methods will be the same.

According to Fig. 5 (b), the permanent magnet can be replaced by a magnetic material with the same permeability and geometric dimensions and a virtual coil with the ampere turns as follows:

$$F = (Ni)_{equiv} = -H_c' \times d \tag{7}$$

The equivalent magnetic resistance of the permanent magnet and the air gap magnetic resistance R_1 and R_2 can be expressed respectively as:

$$R_m = \frac{d}{u_r \times S_1}, \quad R_1 = \frac{k_1 \times l_1}{u_0 \times S_1}, \; R_2 = \frac{k_2 \times l_2}{u_0 \times S_2} \tag{8}$$

where k_1 and k_2 are used to characterize the edge flux effect of the air gap ($k_1, k_2 < 1$). The magnetic induction intensity and magnetic flux can be derived from Ohm's law of magnetic circuit:

$$\varphi = \frac{F}{R_M} \tag{9}$$

where R_M is the sum of the total magnetic resistance in the magnetic circuit, in the brake PM magnetic circuit.

$$R_M = R_m + R_1 + \frac{1}{2}R_2 \tag{10}$$

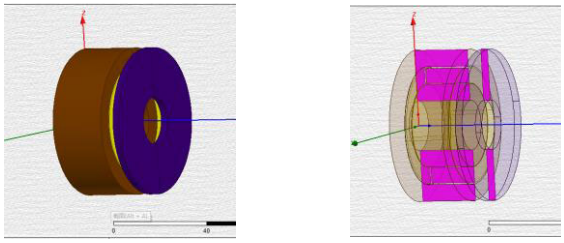

(a) Electromagnet model

(b) Cross section of the model

FIGURE 7. Electromagnet model in Maxwell.

The magnetic field intensity on the air gap l_1 is H_1 and the magnetic field strength on the air gap l_2 is H_2. The total magnetomotive force of the magnetic circuit will be zero, then:

$$H_m \times d = H_1 \times l_1 + H_2 \times l_2 \tag{11}$$

According to the magnetic flux continuity theorem, Eq. 12 can be described as follows:

$$B_m \times S_1 = u_0 \times H_1 \times S_1 = t \times u_0 \times H_2 \times S_2 \tag{12}$$

where the coefficient t is used to denote the large air gap edge flux on surface S_2 in the permanent magnet magnetic circuit. S_2 is smaller than S_1 and t will be larger than 1. Eq. 7 can also be derived from Eq. 11 and Eq. 12:

$$B_m = \frac{B_r}{1 + \frac{1}{d} \times (l_1 + m \times l_2)} \tag{13}$$

where

$$m = t \times \frac{S_1}{S_2} \tag{14}$$

Then the suction force of the permanent magnet on the brake armature can be calculated by the following formula:

$$F = \frac{B_m^2 \times S_1}{2 \times u_0} \tag{15}$$

III. VERIFICATION OF ANALYSIS OF PROPOSED BRAKE MAGNETIC CIRCUIT

The proposed brake magnetic model and calculation method of the electromagnet and the permanent magnet are verified by Maxwell [14]–[19]. The finite element analysis of the electromagnet and the permanent magnet are established respectively.

The volume shape of the electromagnet is consistent with that of the experimental plan and the electrical excitation is 1000 ampere turns. The stroke between the electromagnet and the brake armature is from 0.1mm to 1.5mm. The transient analysis is executed in the software, Figure. 7 shows the electromagnet finite element simulation model and cross-sectional diagram of the electromagnet.

Comparison of the simulated value, the theoretical value and the experimental value of the suction force is given in Fig. 8 (b). The value of the coefficient k is chosen as 0.9 and

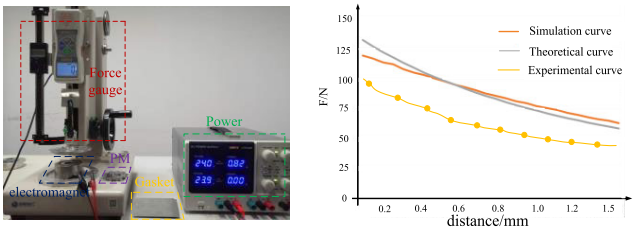

(a).Experimental test platform

(b).Comparison of the electromagnet force

FIGURE 8. Experimental test platform and the electromagnet force comparison results.

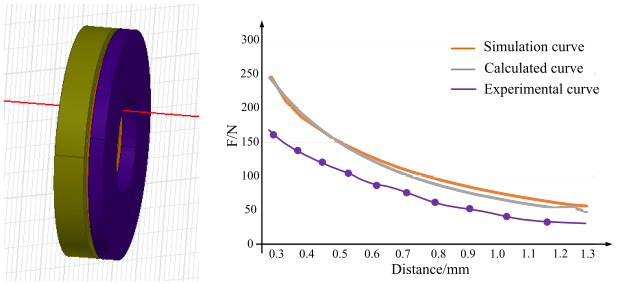

(a) Permanent magnet model

(b) Comparison of the permanent magnet force on the armature

FIGURE 9. The permanent magnet model and comparison of suction force.

the theoretical result is very close to the simulation result. Figure. 8 (a) is the experimental test platform.

In the engineering measurement, the measured electromagnet force value is slightly smaller than the theoretically derived value, which is mainly caused by the following reasons:

1). Measurement error;

2). The actual solenoid coils are not ideal infinitely long straight wires;

According to Fig. 5 (a), a simulation model and experimental test of the permanent magnet is established. A N38 toroidal Nd-Fe-B permanent magnet is used in the simulation and the experimental test. The distance between the permanent magnet and the brake armature is from 0.3mm to 1.3mm. The transient simulation analysis is executed in the software and comparison of the simulated, theoretical and experimental suction force is given in Fig. 9.

The actual amount of magnetization of the experimental permanent magnet is less than the ideal value, so the experimental test result is much smaller. The finite element simulation verifies the magnetic circuit analysis method for electromagnets and the permanent magnet and provides a guide for the analysis of magnetic circuit structures with hybrid excitation (permanent magnet excitation and electrical excitation) [18].

IV. ADVANTAGE OF PROPOSED BRAKE MECHANISM

A. ENHANCED WORKING RELIABILITY

The torque spring is a mechanical part which uses elastic deformation to work. Under normal circumstances, the fatigue life of ordinary springs is between 50,000 and 500,000 times. In the application of space robots, the complex space environment will increase the possibility of spring fatigue failure. Compared to torque springs, there is no physical contact when permanent magnets act on the brake plates, there will be no fatigue failure problem and the working reliability will be enhanced effectively.

B. REDUCTION OF POWER CONSUMPTION

Due to the position relationship between the permanent magnet and the electromagnet, the stroke of the brake armature can be relatively larger than the torque spring brake mechanism which also makes the holding current smaller in

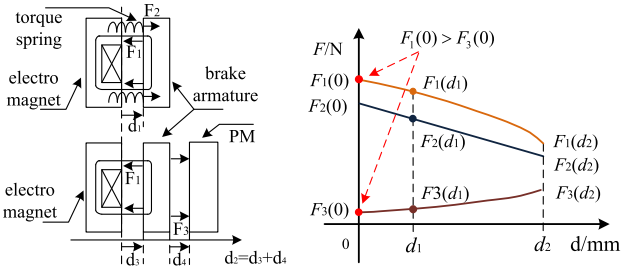

FIGURE 10. Comparison of force analysis between the two brake mechanism.

the electrical holding state. Figure. 10 shows the comparison of the force analysis between the traditional torque spring brake mechanism and the proposed permanent magnet brake mechanism during the initial release state of the brake mechanism after power-on. The relationship between the force and distance as well as the binding relationship between various forces is analyzed. It is assumed that the two types of brake structures have the same electromagnet structure.

In Fig. 10, F_1, F_2, F_3 denotes the suction force of the electromagnet, the torque spring and the permanent magnet on the brake armature respectively. The position where the electromagnet completely pulls in the brake armature is set as zero and the brake armature strokes of the torque spring brake and the permanent magnet brake are expressed as d_1 and d_2.

In order to ensure that the brake mechanism can be released normally after power-on, the force-distance function F_1(d) curve needs to be above the function curve F_2(d). F_1(d) curve obeys the law of exponential decline while the function F_2(d) obeys a linear descent law. So the stroke of the torque spring brake is relatively small, usually 0.1mm while the permanent magnet brake stroke can be 0.5mm to 1mm. The permanent magnet force function F_3(d) obeys a non-linear rise trend. In the process of brake releasing, the torque spring brake and permanent magnet brake meet the following equations:

$$\begin{cases} d_1 < d_2 \\ F_1(d) > F_2(d) \\ F_1(d) > F_3(d) \end{cases} \tag{16}$$

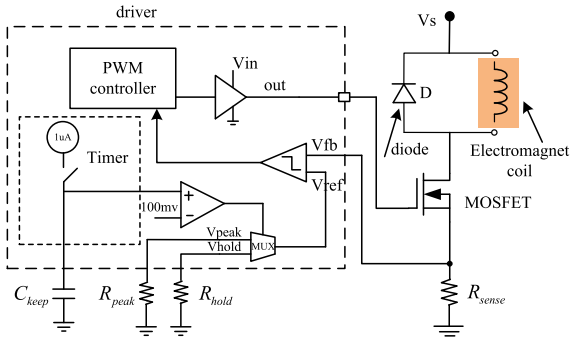

FIGURE 11. Schematic diagram of the conventional brake power supply circuit.

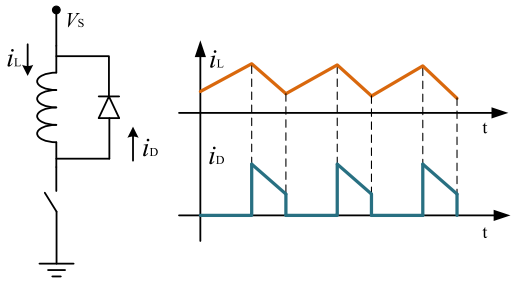

FIGURE 12. Key waveforms of the main power circuit.

After the brake is released, the brake enters the holding state and the stroke is zero at this time. The force of the torque spring and permanent magnet on the brake armature are $F_2(0)$ and $F_3(0)$ respectively. According to Fig. 14 and equation 16, $F_2(0)$ is much larger than $F_3(0)$ which on the other hand means that the holding current of the permanent magnet brake is much smaller than the torque spring brake mechanism.

V. IMPRORVED BRAKE POWER SUPPLY CIRCUIT

The brake power supply circuit is used to control the operation of the electromagnet by adjusting the magnitude of the working current. The working principle of the brake power supply circuit is as follows:

1. Large current excitation of the electromagnet lasting 0.2-1s to release the brake after power on;

2. Small current excitation during the holding state to save energy and reduce heat generation.

Figure. 11 depicts the schematic diagram of the conventional brake power supply circuit [20]–[23].

The circuit is mainly composed of the control circuit, current detection circuit, power MOSFET, freewheeling diode, etc. The electromagnet coil current is controlled to be consistent with the reference value. The reference current value can be adjusted by the capacitor charging time. The electromagnet coil inductor is charged by the voltage source when the MOSFET is turned on, the coil inductor current freewheels through the diode after the MOSFET is turned off. Figure. 12 describes the key waveforms of the main power circuit.

In Figure. 12, the freewheeling diode is clamped at both ends of the inductor, so that the coil inductor current will obey the following equation:

$$L \times \frac{di(t)}{dt} + R \times i(t) + V_D = 0 \tag{17}$$

In the above Eq. 17, i_0 is the initial electromagnet coil current after power-off. R in the formula includes the coil resistance and the diode resistance. The coil current decreases with the exponential rate of R/L. V_{D} is the diode turn on voltage drop. In the robot joint brake mechanism, the electromagnet coil inductance is large enough which requires a relatively long time to consume the stored energy after power off. This will slow down the corresponding speed of the brake mechanism.

In order to improve the corresponding speed of the brake mechanism, the electromagnet coil can be discharged through the power source after power off. The power supply can be equivalent to a charged large capacitor after power off. The electromagnet coil inductance current will obey the following equation in the equivalent capacitor discharge scheme.

$$\mathrm{L} \times \frac{d^2i}{dt^2} + R \times \frac{di}{dt} + \frac{1}{C} \times i = 0 \tag{18}$$

Figure. 13 shows the capacitor discharge scheme and the comparison of the discharging speed between the diode discharge scheme and the capacitor discharge scheme [13].

With the circuit parameters in Fig. 12 (a), the discharging speed of the diode scheme and capacitor scheme can be calculated with MATLAB. When the initial inductor current as 0.5A, the capacitor and diode discharging time is 0.004s and 0.007s.

In order to realize the above-mentioned capacitor discharge scheme, a H-bridge power supply circuit is used to control the electromagnet inductance current of the electromagnet and achieve a rapid discharge speed after power off by connecting the electromagnet coil to the supply power. Fig. 14 shows the H-bridge current paths of the proposed power circuit of the brake circuit. To save costs, the upper left and lower right switches are replaced by diodes.

During the normal operation of the brake power supply circuit, diagram 1 and 2 in Fig. 13 indicate the current path of the electromagnet coil in the forward drive and high-side freewheeling phase respectively. In diagram 1, the upper-left MOSFET and lower-right MOSFET are turned on to drive the electromagnet coil with the power supply voltage applied to the inductor. When the lower-left MOSFET is turned off, the upper-left diode and upper-right MOSFET form a loop to recirculate the electromagnet coil current.

The key part of the proposed H-bridge circuit is the power-off phase. When the power is cut off, the back electromotive force generated by the electromagnet coil inductance will force the upper-left and lower-right diodes to turn on and conduct a current loop through the power supply which is equivalent to the electromagnet connected to a charged capacitor.

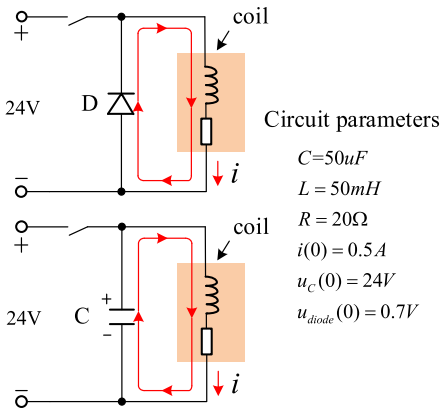

(a) Circuit parameter

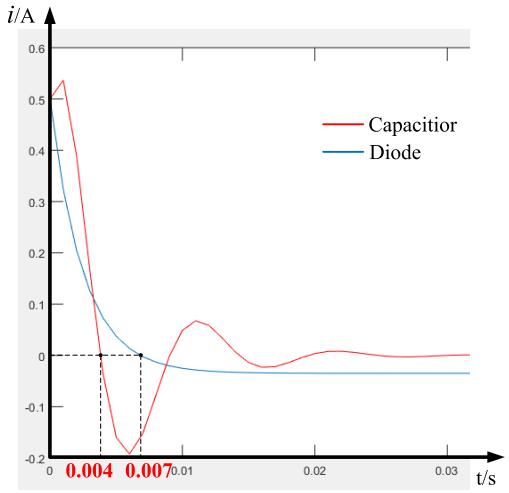

(b) Comparison of discharging speed

FIGURE 13. Capacitor discharging scheme and comparison of discharging speed.

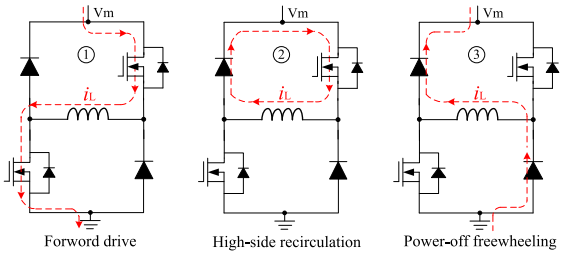

FIGURE 14. Improved H-bridge brake power supply circuit.

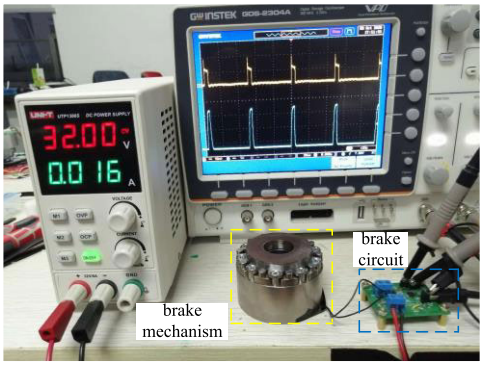

FIGURE 15. Experimental testing platform.

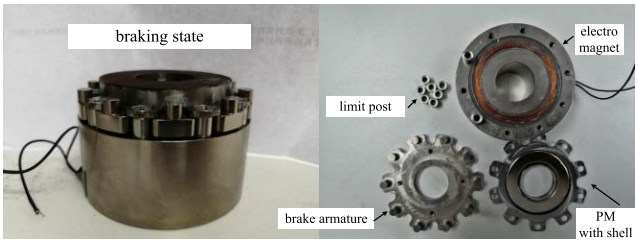

FIGURE 16. Braking state and specific parts of the permanent magnet brake mechanism.

TABLE 2. Structure parameters of the permanent magnet brake.

The electromagnet structure		The permanent magnet structure	
Stroke	1mm	Stroke	1mm
Coil diameter	0.4mm	PM inner diameter	24mm
Coil resistance	28Ω	PM outer diameter	40mm
Coil turns	1000	PM thickness	4mm
Suction force (I=1.2A, d=0mm)	120N	Suction force (d=0.2mm)	40N
Suction force (I=1.2A, d=1mm)	60N	Suction force (d=1mm)	22N

TABLE 3. Parameters of the brake circuit.

Input voltage	32V	Controller	DRV110(TI)
Peak current	1.1A	Switching frequency	20 kHz
Holding current	0.1A	MOSFET Q_1	BSZ22DN20NS3 (Infineon)
Holding time	0.5s	Diode D_2/D_3	SS36(60V/3A)

VI. EXPERIMENTAL VERIFICATION

To verify the functionality of the proposed permanent magnet brake mechanism, a hardware platform is built based on the latch type permanent magnet brake. Figure. 15 shows the photo of the platform.

In Fig. 15, the brake mechanism is keeping in a released state with the brake armature attached on the electromagnet. Fig. 16 shows the braking state of the brake and the specific parts of the permanent magnet brake mechanism.

The electromagnet and the back iron of the permanent magnet along with the brake plates are made of electrical pure iron which has a high magnetic permeability. Nd-Fe-B permanent magnet is used in the brake mechanism, with grant N38. Table 2 lists the parameters of the brake mechanism.

The brake power supply circuit is composed of a solenoid current control chip DRV110 and a peripheral bridge power circuit with two rectifier diodes. Table 3 lists the parameters of the brake power supply circuit.

Figure. 17 is the prototype of the brake power supply circuit. The gate drive signal of MOSFET Q_1 and the voltage on current sense resistor are also given in Fig. 18.

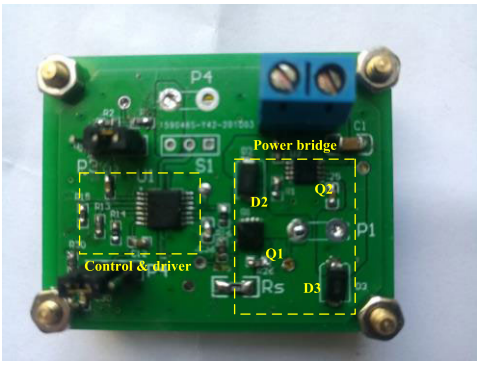

FIGURE 17. Prototype of brake power supply circuit.

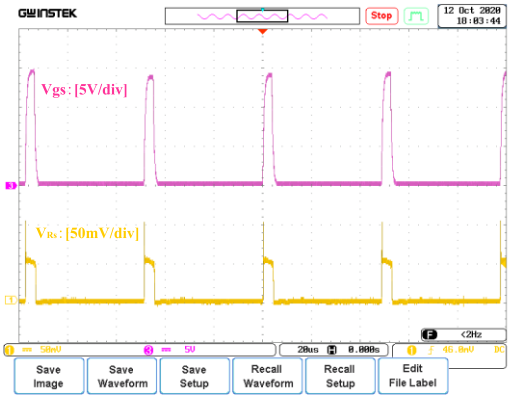

FIGURE 18. Gate drive signal and voltage of current sense resistor of brake circuit.

According to the experimental results, the functionality of the permanent magnet brake is validated and the performance and advantage of the proposed brake mechanism is verified. With the proposed permanent magnet brake mechanism, the holding current can be decreased to 0.1A. This kind of high reliability and low power consumption brake mechanism is suitable for space manipulator environment and provides a useful reference for the design of the manipulator brake mechanism.

VII. CONCLUSION

In order to solve the problems of high power consumption and high temperature rise in the conventional electromagnetic-spring brake mechanism, a novel permanent magnet brake mechanism is proposed. This permanent magnet brake mechanism is suitable for bolt type brake method which can generate a very large braking force. The magnetic circuit models of the electromagnet and permanent magnet are established and verified by the finite element method. The advantage of the low power consumption of the permanent magnet brake mechanism is analyzed. A novel H-bridge brake power supply circuit can effectively accelerate the speed of inductor discharge and improve the corresponding speed of the brake mechanism.

REFERENCES

[1] C. W. Xiong, H. Z. Lv, Y. F. Shu, and S. L. Fan, "Design and simulation analysis of an electromagnetic brake for a robot arm joint," *Mech. Res. Appl.*, vol. 32, no. 1, pp. 171–173, Feb. 2019.

[2] T. Yoko, T. Takeshita, and H. Arakawa, "Brake control apparatus obtaining braking force by pressing of friction member using motor," U.S. Patent 6 845 582 B2[P], Mar. 19, 2003.

[3] Y. Konishi and S. Kuragaki, "Electric braking apparatus and method of controlling thereof," EP Patent 1 892 164 A2[P], Feb. 27, 2008.

[4] M. E. Kimble, "Electromagnetic spring-actuated brake system," U.S. Patent 6 439 355 B1[P], Aug. 27, 2002.

[5] J. Bigeon, J. Sabonnadiere, and J. Coulomb, "Finite element analysis of an electromagnetic brake," *IEEE Trans. Magn.*, vol. MAG-19, no. 6, pp. 2632–2634, Nov. 1983.

[6] K. S. Schroeder, "Electromagnetic brake/clutch," U.S. Patent 5 713 444, Feb. 3, 1983.

[7] Y. J. Shin, K.-S. Kim, and S. Kim, "Development of electromagnet brake robot finger for highly dexterous motion through a single motor," in *Proc. IEEE Veh. Power Propul. Conf.*, Oct. 2014, pp. 1423–1426.

[8] J.-Y. Choi, S.-Y. Sung, S.-M. Jang, and S.-H. Lee, "Design and dynamic analysis of magnetically levitated electromagnets with low-resolution position sensor," *IEEE Trans. Magn.*, vol. 48, no. 11, pp. 4546–4549, Nov. 2012.

[9] R. Saini, "Optimal design and analyses of T-shaped rotor magnetorheological brake," in *Proc. IOP Conf. Mater. Sci. Eng.*, Oct. 2019, Art. no. 012024.

[10] T. Yamaguchi, Y. Kawase, T. Nakano, T. Asano, R. Kawai, and T. Takemoto, "Electrical loss analysis of AC electromagnet with shading coil taking into account eddy current in laminated cores," *IEEE Trans. Magn.*, vol. 50, no. 2, pp. 957–960, Feb. 2014.

[11] M. R. Cheng, "Discussion on application conditions of Ampere's Loop Theorem," *J. Higher Corresp. Education.*, vol. 19, no. 6, pp. 42–44, Dec. 2006.

[12] S. D. Umans, *Electric Machinery*. Beijing, China: Publishing House of Electronics Industry, 2013.

[13] Q. Wang, J. B. Zou, and X. H. Fu, "Calculation method of permanent magnet magnetic co-energy," *Trans. China Electrotech. Technol.*, vol. 25, no. 5, pp. 25–30, May 2010.

[14] Y. Kawase, T. Yamaguchi, and K. Iwashita, "3-D finite element analysis of dynamic characteristics of electromagnet with permanent magnets," *IEEE Trans. Magn.*, vol. 42, no. 4, pp. 2632–2634, Apr. 2006.

[15] Y. Bakhvalov, V. Grechikhin, O. Kravchenko, and A. Yufanova, "Optimal design of shell-type electromagnets of XY-coordinate electric actuator," in *Proc. 9th Int. Conf. Power Drives Syst. (ICPDS)*, Oct. 2016, pp. 1–4.

[16] G. Q. Liu, L. Z. Zhao, and J. Y. Jiang, *Finite Element Analysis of Engineering Electromagnetic Field Based on Ansoft*. Beijing, China: Publishing House of Electronics Industry, 2005.

[17] Y. B. Wang, B. Xu, and Y. J. Liu, "Simulation analysis of the dynamic characteristics of the solenoid based on Ansoft and AMESim," *Mach. Tool Hydraulcs*, vol. 36, no. 9, pp. 104–105, 2008.

[18] S. N. Cai, C. T. Xu, and L. Yu, "Optimizing design of magnetic circuit for a self-holding micro electromagnet," in *Proc. Int. Conf. Electr. Inf. Control Eng.*, Apr. 2011, pp. 6005–6008.

[19] Q. F. Li, *Numerical Calculation of Electromagnetic Fields and Design of Electromagnets*. Beijing, China: Tsinghua University Press, 2002.

[20] V. Blasko, "Power conditions and control of a regenerative brake," in *Proc. Conf. Rec. IEEE Ind. Appl. Conf. 33rd IAS Annu. Meeting*, vol. 2, Oct. 1998, pp. 1504–1510.

[21] J. Jiang and J. Holtz, "An efficient braking method for controlled AC drives with a diode rectifier front end," *IEEE Trans. Ind. Appl.*, vol. 37, no. 5, pp. 1299–1307, Sep. 2001.

[22] A. Weissman, "Motor braking arrangement and method," U.S. Patent 4 250 436 B1[P], Feb. 10, 1981.

[23] Y. H. Wang, "Inductance coil fast discharge circuit," C.N. Patent 2 01 966 816 U Sep. 7, 2011.

KAIMENG WANG is currently pursuing the M.Eng. degree with the College of Astronautics Engineering, Nanjing University of Aeronautics and Astronautics, Nanjing, China. His research interests include robot structure design, motor control, and space robot force control.

HEHUA JU received the Ph.D. degree in aircraft design from the Harbin Institute of Technology, in 2003. He is currently a Distinguished Professor with the College of Astronautics, Nanjing University of Aeronautics and Astronautics. His research interests include autonomous robotics, lunar rover motion planning and control, deep space probe research, and spacecraft design.

YANG YANG received the master's degree from the Nanjing University of Aeronautics and Astronautics, Nanjing, China, in 2016, where he is currently pursuing the M.Eng. degree with the College of Astronautics Engineering. His research interests include novel motor design, motor control, and robot design.

ZHENHAO GUO is currently pursuing the M.Eng. degree with the College of Astronautics Engineering, Nanjing University of Aeronautics and Astronautics, Nanjing, China. His research interests include the inverse kinematics and motion planning for robot-arms with high degree of freedom.